

Numerical modelling of fire test with timber fire protection

Numerical
modelling of
fire test

Vojtěch Šálek

*Department of Chemical Engineering, University of Chemistry and Technology,
Prague, Czech Republic*

Kamila Cábová and František Wald

*Department of Steel and Timber Structures, Czech Technical University in Prague,
Prague, Czech Republic, and*

Milan Jahoda

*Department of Chemical Engineering, University of Chemistry and Technology,
Prague, Czech Republic*

99

Received 16 April 2021
Revised 28 July 2021
Accepted 22 August 2021

Abstract

Purpose – The purpose of this paper is to present a complex pyrolysis computational fluid dynamics (CFD) model of timber protection exposed to fire in a medium size enclosure. An emphasis is placed on rarely used temperature-dependent thermal material properties effecting the overall simulation outputs. Using the input dataset, a fire test model with oriented strand boards (OSB) in the room corner test facility is created in Fire Dynamics Simulator (FDS).

Design/methodology/approach – Seven FDS models comprising different complexity approaches to modelling the burning of wood-based materials, from a simplified model of burning based on a prescribed heat release rate to complex pyrolysis models which can describe the fire spread, are presented. The models are validated by the experimental data measured during a fire test of OSB in the room corner test facility.

Findings – The use of complex pyrolysis approach is recommended in real-scale enclosure fire scenarios with timber as a supplementary heat source. However, extra attention should be paid to burning material thermal properties implementation. A commonly used constant specific heat capacity and thermal conductivity provided poor agreement with experimental data. When the fire spread is expected, simplified model results should be processed with great care and the user should be aware of possible significant errors.

Originality/value – This paper brings an innovative and rarely used complex pyrolysis CFD model approach to predict the behaviour of timber protection exposed to fire. A study on different temperature-dependent thermal material properties combined with multi-step pyrolysis in the room corner test scenario has not been sufficiently published and validated yet.

Keywords Fire protection, Pyrolysis, Complex modelling, Room corner test, FDS, Input parameters, OSB, Validation

Paper type Research paper

1. Introduction

Protection of steel elements with timber can be a very efficient way of increasing their fire resistance. Thus, the reliable prediction of the temperature environment in a fire compartment with such a structure should be investigated. When a structural element is protected with timber, the prediction of surrounding temperature is even more complicated as fire protection serves as the supplementary source of fire at one time. There are many alternative passive fire protection systems for reducing the rate of temperature rise in structures exposed to fire. Typical fire protection materials covering calcium silicate or gypsum boards, cement-based sprays with glass or cellulosic fibrous reinforcing or intumescent paints are demanding on



Journal of Structural Fire
Engineering
Vol. 13 No. 1, 2022
pp. 99-117

© Emerald Publishing Limited
2040-2317
DOI 10.1108/JSE-04-2021-0017

This work was supported by The Czech Science Foundation (GACR) through Project No. 19-22435S, and the grant of Specific university research – grant No. A1_FCH_2020_004. The authors would like to thank Msc. Filip Zeman for constructive suggestions and comments.

production time, production cost and energy. Timber-based materials have experienced a renaissance during the recent few decades due to their environmental credentials and societal goals striving for sustainable development with lower energy demands and less pollution in all sectors, including the construction sector that stands for a significant part of the overall community economy. Thanks to the extraordinary behaviour of timber when exposed to fire, which burned part becomes a layer char insulating the raw materials below it, it is possible to provide fire protection to steel elements with timber boards or heavy timber. It was already shown by [Twilt and Witteveen \(1974\)](#) that 35 mm thick softwood boards can provide fire resistance for 60 min to a steel member with section factor 100 m^{-1} .

Computational fluid dynamics (CFD) modelling, commonly used in fire safety engineering to predict the temperature environment during fire conditions, may also predict the temperature environment around a structural element protected with timber. In this case, it is even more complicated as the fire protection serves as the supplementary source of fire at one time. When the timber material is exposed to fire, the surface of the material ignites and burns rapidly. There is a process of pyrolysis, in which flammable gases are released from the timber, which then burns and the heat generated acts on the timber material and the environment. The burned timber becomes a layer of char that insulates the solid, and the burning rate decreases ([Buchanan et al., 2014](#)). Fluid dynamics of hot gases is a complex problem that depends on many factors, see [Drysdale \(2011\)](#). The accuracy of the mathematical solution is based on entering the complete range of input data. The most problematic task lies in the accurate modelling of the fire source. When the structural element is protected with timber, the protection serves as a fire load at one time. Model of thermal degradation of wood has to be implemented into CFD model.

CFD modelling of the burning timber may be simulated using different approaches. From the simplified model of burning based on the prescribed heat release rate, via the description of pyrolysis using one-step reaction, up to the complex description of pyrolysis. A commonly used simplified approach is not sufficient for fire spread predictions which remain an ongoing challenge within the fire safety community. Complex pyrolysis models based on physical and chemical processes existing during solid material burning can theoretically describe the fire spread. However, publications on the complex pyrolysis approach and its applications in medium size fire scenarios (e.g. room corner test), where the fire spread occurs, are nearly missing. The problem lies in the values of input parameters that are needed for complex modelling. Their obtaining is not an easy task.

Mathematical description of physical and chemical processes ongoing during pyrolysis comprises solid material decomposition according to a simplified thermal decomposition reaction scheme, the kinetics of thermal decomposition, heat and mass transport, char creation, combustion, etc. Implementing these processes leads to a large input parameter set needed to describe the thermal and kinetic material behaviour. The input parameters, especially kinetic parameters, are very difficult or impossible to find in the literature, and some have to be obtained experimentally. Even when a complete input dataset is collected, its transferability into CFD based model is little known and questionable due to model-dependent parameters obtained via optimization routines from experimental data. Nevertheless, the complex pyrolysis approach, including all challenges connected with input parameters, offers an opportunity to replace the commonly used simplified model in scenarios where the simplified procedure is insufficient.

This study aims to collect known material input parameters from the literature and experimentally measure or estimate the missing parameters to create a complete input dataset that is needed for building a complex pyrolysis CFD model with structural element protected with timber. Using the input dataset, a fire test in the room corner test facility with oriented strand boards (OSB) serving as fire protection is created in Fire Dynamics Simulator (FDS).

2. Current state

2.1 Literature overview

The first attempt to mathematically describe the heat release rate in room corner tests with combustible lining materials presents [Karlsson \(1992\)](#). The author presented an analytical solution that is based on a thermal theory for flow flame spread. The solution uses a simple representation of the heat release rate from a cone calorimeter.

In recent years, numerical modelling of burning room corner test using an advanced approach has been addressed only in a few research works. [Hietaniemi et al. \(2004\)](#) presented case studies of fire experiments executed in a room corner test facility where the burning item including spruce timber, MDF board, PVC carpet and others is made up of the linings of a room. Input parameters governing the pyrolysis and combustion of solid materials were given from the small-scale cone calorimeter results. Data obtained in the experimental set up were compared with results of the numerical model conducted in FDS 4.0. Heat transfer and pyrolysis inside the charring materials were modelled using a one-dimensional model. The pyrolysis was assumed to occur on an infinitely thin front, moving inside the material instead of the continuous pyrolysis region. Although the study has unveiled some discrepancies in the FDS program results and the measured results, the importance of the research on this topic is definite. A similar level of modelling of burning was presented in the thesis of [Buchnarova \(2018\)](#). The author presented the experimental and numerical study of wood-based materials in a cone calorimeter and room corner test facility. A simplified model of cone calorimeter created in FDS was used to calculate the heat release rate from a wood-based board. Material parameters of the board were obtained from thermogravimetric analysis (TGA). Then the model with temperature dependant material characteristics was studied. In this study, the room corner fire test with wood-based material was also simulated in FDS. Material characteristics obtained from cone calorimeter tests were used for this model. Except for the definition of burning by heat release rate, an approach of modelling using one pyrolysis reaction divided into two steps was presented. Results of pyrolysis were described using the rate of C-H-O and soot. Kinetic constants were taken from TGA. The importance of the specimen orientation during the cone calorimeter test, non-uniform heat flux during the room corner test and the difference of specimen sizes in both tests were discussed in this study's conclusions. An advanced approach to modelling the burning was also used in [Brunkhorst and Zehfuss \(2020\)](#). The paper deals with the experimental and numerical test in a compartment with combustible surfaces. The tests were conducted in a corner test room with timber surfaces. A numerical analysis in FDS 6.7 simulating the burning used two approaches to modelling timber burning: modelling a predefined time-dependent heat release rate (HRR) based on test results and modelling a one-dimensional pyrolytic decomposition of timber. The pyrolysis of wood was modelled by a simple one-step solid phase reaction (wood – char). The study showed that the model with predefined HRR underestimates the test results. The model with one-step pyrolysis was not prosperous, and it did not ignite the fire load.

Due to the pyrolysis modelling complexity, a simplified solution based on simulation of burning using a prescribed heat release rate is applied in most research papers. [Moghaddam et al. \(2004\)](#) presented a numerical simulation of a room corner fire in FDS. The simulation of a corner fire with plywood as combustible wall linings and without combustible wall linings was compared to published experiments. The burning of plywood was described using combustion parameters (ignition temperature, heat of gasification and heat of combustion) coming from literature. The study included mesh sensitivity analysis, which showed a suitable grid size to accurately reproduce the gas temperature inside the room. [Moinuddin et al. \(2011\)](#) also used the simplified way of simulation of burning. The paper presents a numerical and experimental study of gas temperature rise during a room corner. The experimental programme includes protected and unprotected steel elements to study steel

temperature. Burning in the numerical model conducted in FDS 5.3 was simulated with the aid of prescribed HRRs obtained from experimental data. The same modelling approach is used in the paper by [Lattimer et al. \(2019\)](#). A numerical research model of the room corner test in FDS 6.4 was applied to study the flammability requirements for interior finish materials used in rail cars. In the model, fire growth was predicted using the heat release rate per unit area (HRRPUA) and ignition temperature. HRRPUA was obtained from cone calorimeter test data. Similarly, [Beshir et al. \(2019\)](#) presented the heptane pool fire model using the prescribed heat release rate. In the study, reduced-scale and full-scale room corner fire tests were simulated in FDS to demonstrate the window location's effect.

2.2 Approaches to numerical modelling

FDS allows describing the pyrolysis of a solid material either via a simple or complex pyrolysis model. In the simple pyrolysis model, the given material's burning description based on its properties is replaced by a defined value of heat release rate per unit area (HRRPUA). Once the ignition temperature is reached, the described material becomes essentially a burner ejecting gaseous fuel. The amount of discharged gaseous fuel, \dot{m}_j to produce the user specified HRRPUA, \dot{q}_{user} is computed according to the equation:

$$\dot{m}_j = f(t) \dot{q}_{user} / \Delta H_C,$$

where $f(t)$ denotes the time ramp and ΔH_C gas phase heat of combustion ([McGrattan et al., 2019a](#)). Ignition temperature, HRRPUA and time ramp are the only three parameters required to define burning in a simplified pyrolysis model apart from the thermal material properties needed to solve one-dimensional heat transfer to reach the ignition temperature.

In the complex pyrolysis model, the burning rate of each solid material i undergoing one or more reactions j is computed from kinetic equation ([McGrattan et al., 2019b](#)):

$$dY_{s,i}/dt = - \sum_{j=1}^{N_{r,i}} r_{ij} + \sum_{l'=1}^{N_m} \sum_{j=1}^{N_{r,l'}} \nu_{s,l'j} r_{l'j} (l' \neq i); Y_{s,i} = (\rho_{s,i} / \rho_s(0)),$$

where $\rho_{s,i}$ and $\rho_s(0)$ represent the density of i th material component and initial density, respectively. The second term on the right side represents the contribution of other materials producing the i th material with a yield of $\nu_{s,l'j}$. The reaction rate, r_{ij} at the temperature, T_s , obtained by solving one-dimensional heat transfer, is defined as ([McGrattan et al., 2019b](#)):

$$r_{ij} = A_{ij} Y_{s,i}^{n_{s,ij}} \exp\left(-\frac{E_{ij}}{RT_s}\right) X_{O_2}^{n_{O_2,ij}}.$$

Each material component undergoing decomposition, therefore, requires kinetic parameters A – pre-exponential factor, E – activation energy and n – reaction order have to be specified. The heterogeneous reaction order, $n_{O_2,ij}$ represents oxidation reactions.

3. Room corner test model

A set of room corner test (RCT) models was created in FDS version 6.7.4 based on an experiment carried out by the University Centre for Energy Efficient Buildings CTU in Prague (UCEEB). The experiments were performed in a room corner test facility according to [ISO 9705-1 International Standard \(2016\)](#). Wood-based material, specifically OSB, was used as a lining of the testing room. The experiments serve both as a basis to create the FDS model and as a data source for the model validation.

The set of created RCT models comprises seven different OSB fire behaviour definition settings, marked Scenario A to G. In Scenario A, the OSB burning is prescribed using the simplified FDS pyrolysis model. In Scenarios B to G, the complex FDS pyrolysis model including OSB thermal decomposition kinetics description with different thermal properties of OSB is used. Different specific heat capacity (c_p), and heat conductivity (k) values of OSB are selected as follows: Scenario B – both constants c_p and k specified by the manufacturer, Scenario C – both temperature dependent c_p and k , Scenario D – both temperature-dependent c_p and k with neglected water evaporation, Scenario E – constant c_p and temperature-dependent k , Scenario F – constant k and temperature-dependent c_p , Scenario G – constant k and temperature dependent c_p with neglected water evaporation. Both temperature-dependent c_p and k are taken from EN 1995-1-2 Eurocode 5 (2006). The summary of each scenario set is shown in Table 1.

3.1 CFD model description

3.1.1 Geometry, mesh, initial and boundary conditions. The computing domain is based on the room corner test geometry defined in ISO 9705-1 International Standard (2016). The geometry consists of the fire test room (length 3.6 m, width 2.4 m, height 2.4 m) with a doorway (width 0.8 m, height 2.0 m) in the centre of the short room wall. The outer space (length 3.0 m, width 3.0 m, height 4.5 m) is adjoined to the doorway. The whole model geometry can be seen in Figure 1.

Three different mesh resolutions (low, medium and high) of the whole model geometry are proposed to evaluate the model results sensitivity on cell size. Each mesh is further divided into four submeshes: submesh 1 – fire test room; submesh 2 – space directly in front of the doorway (length 1.5 m, width 3.0 m, height 2.4), submesh 3 – space above submesh 2; submesh 4 – the rest of outer space. Mesh division is presented in Figure 1. Submeshes are introduced to save computational time using MPI (Message Passing Interface) parallelization, which requires splitting the domain into multiple meshes. All the mainly observed processes of fire development occur inside the fire test room. However, gas flow in the vicinity of the doorway can significantly affect the course of fire development as the fully developed fire stage becomes ventilation driven. Therefore, the resolution of both submeshes 1 and 2 is tested. Different cell sizes and the total number of cells in each submesh are shown in Table 2.

The ceiling, floor and the three fire test room walls at the edge of the model domain are solid boundaries with backing set as “void”. This setting computes the heat transfer coefficient of the wall side facing the exterior from the ambient air properties. The outer space model boundaries are open to ambient air. The initial air composition, temperature, pressure and velocity are left default.

3.1.2 Solid objects geometry. A burner (length 0.2 m, width 0.2 m, height 0.2 m) is placed in the fire test room on the floor in a corner opposite the doorway wall. A hood covering the whole 3.0×3.0 m outer area with an exhaust duct (width 0.3 m, height 0.3 m) is placed in front

Scenario	Pyrolysis	c_p	Evaporation included in c_p	k
A	Simple	Constant	No	Constant
B	Complex	Constant	No	Constant
C	Complex	Temperature dependent	Yes	Temperature dependent
D	Complex	Temperature dependent	No	Temperature dependent
E	Complex	Constant	No	Temperature dependent
F	Complex	Temperature dependent	Yes	Constant
G	Complex	Temperature dependent	No	Constant

Table 1.
The summary of model
Scenario A–G settings

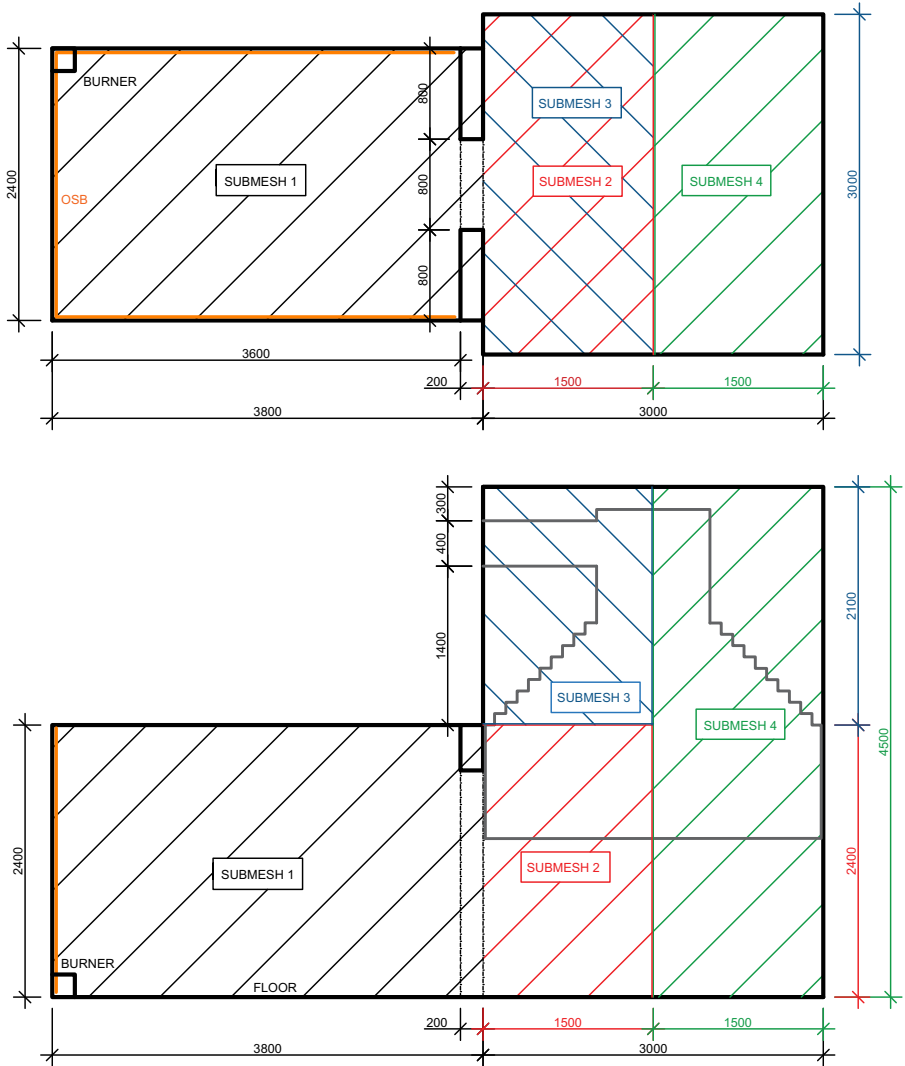


Figure 1.
The overview of RCT model geometry including submeshes are shown. Floor plan (upper picture) and side plan (lower picture)

Mesh	Low mesh resolution		Medium mesh resolution		High mesh resolution	
	Number of cells	Cell size [mm]	Number of cells	Cell size [mm]	Number of cells	Cell size [mm]
Submesh 1	21,888	100	175,104	50	590,976	33.3
Submesh 2	10,800	100	86,400	50	291,600	33.3
Submesh 3	9,450	100	9,450	100	9,450	100
Submesh 4	20,250	100	20,250	100	20,250	100
Total	62,388	-	291,204	-	912,276	-

Table 2.
A comparison of cell sizes and numbers in each submesh for different mesh resolutions

of the doorway to collect all combustible products leaving the fire test room. The hood is composed of dozens of small planar plates as FDS allows only rectangular objects to enter the computational domain. The hood plates cover the outer space from a height of 1.4 meters (except the doorway) and begin to approximate the conical shape from a height of 2.4 meters. The centre of the exhaust duct is at the height of 4.0 meters. The detailed hood and exhaust duct geometry can be seen in [Figure 1](#). A 0.2 m thick wall with the hole to create the doorway is placed between the fire test room and the outer space.

3.1.3 Solid object surfaces. FDS assigns the physical and chemical properties of solid objects by defining the object surfaces. Three different material surfaces are used in RCT simulation – 0.1 m thick concrete wall, 0.115 m thick concrete wall covered by OSB (0.015 m of OSB and 0.1 m of concrete) and an inert surface. The concrete surface is assigned to the fire test room floor, ceiling, wall with the doorway (both inner and outer side of the wall), outer space floor and burner (apart from the top side). The concrete wall covered by OSB surface is assigned to the remaining three fire test room walls. The inert surface is used to define the hood and exhaust duct.

FDS allows each surface to consist of multiple materials, thus giving the opportunity to create a multicomponent surface. The concrete walls used in the model are composed of pure aerated concrete. OSB consists of three individual fictive materials, further referred as cellulose, hemicellulose and lignin, which corresponds to the basic chemical components forming wood. Cellulose, hemicellulose and lignin in OSB are in a weight ratio of 0.398, 0.348 and 0.254, respectively. The OSB component weight ratios are computed from thermogravimetric experimental data by mathematical optimization tools in FDS User's Guide ([McGrattan et al., 2019b](#)). The presence of three main wood chemical components corresponds to the parallel three-step solid material thermal decomposition reaction scheme of OSB as follows:

Solid OSB component 1 (Lignin) $\rightarrow \nu_{\text{char}} \text{Char} + \text{Combustible gases}$,

Solid OSB component 2 (Cellulose) $\rightarrow \nu_{\text{char}} \text{Char} + \text{Combustible gases}$,

Solid OSB component 3 (Hemicellulose) $\rightarrow \nu_{\text{char}} \text{Char} + \text{Combustible gases}$,

where ν_{char} denotes the char yield (kg/kg).

The solid objects inner discretization for heat conduction computation was changed from the default setting for the concrete walls covered by the OSB. An equidistant discretization and an increased number of computational points up to approximately 100 are used. Discretization changes are necessary to eliminate numerical instabilities occurring primarily when the complex pyrolysis approach and temperature-dependent thermal properties are used. All other surfaces discretization apart from OSB covered walls were left default.

In Scenario A, where the FDS simple pyrolysis model is used, an HRRPUA ramp taken from cone calorimetry measurements at 80 kW ([Ira et al., 2020](#)) was added to the surface definition.

3.1.4 Solid materials properties. Five different solid materials, lignin, cellulose, hemicellulose, aerated concrete, and char, were defined. Lignin, cellulose and hemicellulose thermal properties for Scenarios A to G and kinetic properties for Scenarios B to G can be seen in [Table 3](#). Kinetic properties for Scenario A are not listed as the FDS simple pyrolysis model instead of the complex pyrolysis model is used in Scenario A. In the table, ΔH_R values are obtained from DSC measurements in nitrogen atmosphere and correspond to the area of OSB decomposition peak. Kinetic parameters (A , E , n), ρ , ΔH_C and ν_{CHAR} values are taken from the literature ([Ira et al., 2020](#)). Specific heat capacity and heat conductivity values are taken from the Kronospan OSB manufacturer. Note that the influence of the OSB thickness is not tested in this work. However, the thermal parameters provided by the manufacturer cover wide

Figure 2. OSB HRRPUA dependency on time from cone calorimetry measurement with approximated HRRPUA ramp used in FDS model

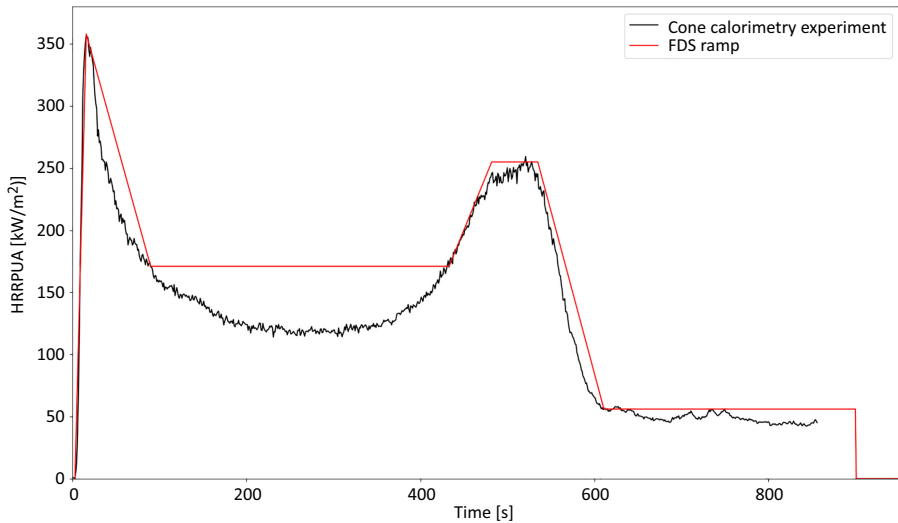


Table 3. Model input parameters of cellulose, hemicellulose and lignin material

Material	$\log A$ [log 1/s]	E [kJ/mol]	n [-]	ρ [kg/ m ³]	c_p [kJ/ mol]	k [W/ (m·K)]	ΔH_R [kJ/kg]	ΔH_C [kJ/kg]	ν_{CHAR} [-]
Cellulose	7.6	112	1.2	587	1.221	0.098	77.7	11,710	0.236
Hemicellulose	25.4	326	1.5	587	1.221	0.098	77.7	11,710	0.236
Lignin	2.7	56	3.1	587	1.221	0.098	77.7	11,710	0.236

range of thicknesses and the kinetic parameters obtained from a well homogenized OSB powder describe the material independently of thickness. It is therefore assumed that it is possible to use the above-mentioned parameters for different OSB thicknesses of similar density.

In Scenarios C to G, the specific heat capacity and/or heat conductivity constant values in Table 3 are replaced by temperature-dependent values from the standard (EN 1995-1-2 Eurocode 5, 2006). The values in EN 1995-1-2 are valid for solid wood. Although the wood structure is different from OSB, wood temperature-dependent thermal properties are very similar to OSB, especially at temperatures below thermal decomposition. Therefore, wood properties are used knowing that it does not significantly affect the initial stage of heating and fast transition into flashover, which is the part on which the comparison with the experiment is focused.

The decomposition reaction of lignin, cellulose and hemicellulose produces combustible gaseous products and solid char. The char density of 299 kg/m³, the specific heat capacity of 0.8 kJ/(K·kg) and heat conductivity of 0.1 W/(m·K) are taken from Gupta *et al.* (2003), who studied the thermal properties of softwood char. Constant char thermal properties are used in Scenario B. When the temperature-dependent heat conductivity and/or specific heat capacity of OSB components are used (Scenario C to G), the char thermal properties are assumed to be equal to the virgin OSB temperature-dependent properties. In Scenario C to G the same temperature dependency is therefore used for both virgin OSB and created char. This assumption is done regarding the course of experimental measurements used to determine

OSB thermal properties, where the measured sample decomposes and creates char during the measurement. Experimental values measured at high temperatures then correspond to char, which replaced the original material during the experiment. This assumption is valid only in cases where char occurs in the model at high temperatures and was not present during the initial heating of virgin material below the temperature of thermal decomposition. Both virgin OSB and char specific heat capacity and heat conductivity in specific scenarios are shown in Figure 3.

Aerated concrete thermal parameters (density of 500 kg/m^3 , specific heat capacity of $1.0 \text{ kJ/(K}\cdot\text{kg)}$ and conductivity of $0.12 \text{ W/(m}\cdot\text{K)}$) remain the same and constant for all Scenarios A to G. The aerated concrete thermal properties are chosen with respect to the average aerated concrete properties. No thermal reactions in char and aerated concrete are assumed. As a result, the kinetic parameters of thermal decomposition reaction are given only for lignin, cellulose and hemicellulose.

During pyrolysis process it is assumed that near the pyrolysis zone oxygen is locally consumed by burning and oxidative reactions are neglected. Therefore, the heterogeneous reaction order, $n_{O_2,ij}$ is left zero (default value) in this study as the reaction rate of thermal decomposition is unaffected by the local oxygen volume fraction, X_{O_2} .

3.1.5 Ignition and combustion. The ignition of OSB covering the walls is achieved by the burner in the fire test room. The burner should be set to a net heat output of 100 kW during the first 10 min of the simulation and 300 kW for a further 10 min according to [ISO 9705-1 International Standard \(2016\)](#). The RCT test is terminated either after 20 min or when a flashover occurs. In the described experiment with OSB, a flashover was reached in 412 s. At 413 s, the experiment was terminated by turning off the burner, closing the fire test room and activating a stable fire extinguisher inside the test room. Therefore, the burner's heat inserted into the FDS simulation via a surface with a predefined HRRPUA ramp covers only the first 412 s. No additional heat from the burner is inserted into the simulation for the rest of the simulation.

In Scenario A an ignition temperature of 232°C is added to the OSB surface definition to initiate the FDS simple pyrolysis model burning. The ignition temperature value is estimated

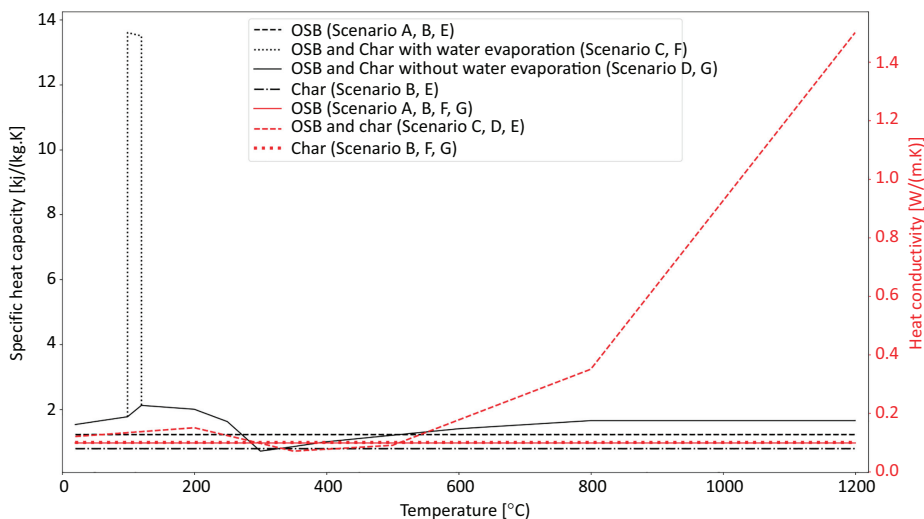
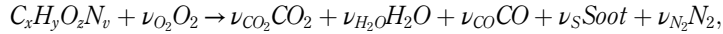


Figure 3.
The dependency of heat conductivity and specific heat capacity on temperature used in each model scenario

based on OSB Safety Data Sheet (Weyerhaeuser, 2018), and the thermal decomposition starts at TGA curve given in thesis (Šálek, 2018).

FDS mixing-controlled combustion model comprises only one reaction of combustible fuel in the gas phase. A simple chemistry model is chosen, where a single-step reaction is assumed to be of the form (McGrattan *et al.*, 2019b):



where ν denotes the stoichiometric coefficients. Stoichiometric coefficients, apart from soot, are computed from the fuel formula, which is estimated as $C_{6.3}H_{9.786}N_{0.041}O_{4.241}$. The estimation is based on wood composition. The fuel molecule size in the sense of carbon content is preserved, and the remaining components (H , O and N) are computed to comply with the relative ratio of OSB elementary composition (Ira *et al.*, 2020). A soot yield value of 0.0075 is used based on cone calorimetry measurements (Ira *et al.*, 2020).

3.1.6 Other parameters. The end of the simulation is set to 30 min due to the estimation of temperature development in a later time. The exhaust duct outlet boundary is replaced by a volume flow ramp of gas species placed as a vent 0.1 m in front of the computational domain boundary. The ramp is based on the volume flow time dependency measured during the experiment.

If some FDS commands are not explicitly mentioned in the previous text, its value is left default.

3.1.7 Devices. The type and location of devices in the FDS model follow their real location during the fire experiment and the suggestions in ISO 9705-1 International Standard (2016). Six coated thermocouples with bead diameter 1.5 mm (corresponds to MAVIS MTC11-E1-4000-50-10) are placed to measure the ceiling surface temperature (labelled as TC8 – TC13). Seven cable thermometers with bead diameter 0.08 mm (corresponds to OMEGA 5TC-TT-K-40) measure the gas temperature in the corner opposing to the burner in heights 670, 970, 1,270, 1,420, 1,570, 1720 and 2,100 mm (labelled as TC1 – TC7). The location of thermocouples in the test room, and identically in the model, can be seen in Figure 4.

3.2 Results and comparison

3.2.1 Mesh sensitivity. The RCT mesh resolution test was evaluated using the results of the time–temperature curve calculated by thermocouple TC7. The results are shown in Figure 5. All three mesh densities show a similar course affected, especially in the first 400 s, by the output temperature noise. The 50 mm mesh fits the course of the 33 mm mesh better than the 100 mm mesh. Simultaneously, the difference between the 50 mm and 33 mm grid spacing is insignificant in comparison to the temperature differences in Scenarios A to G. Therefore, a medium-density mesh with 50 mm grid spacing is chosen for further computations as a compromise between the model accuracy and computational time.

3.2.2 Temperature profiles. The overall behaviour of the model Scenarios A to G is presented in Figure 6. In this figure, the gas temperatures calculated at thermocouple TC7 in FDS models are compared to the gas temperature measured in the same location during the experiment (in Figure 6 denoted as Experiment UCCEEB). Note that the fire test was terminated as described in chapter 3.1.5. Therefore, the experimental thermocouple output ends at 412 s. The comparison of thermocouple temperatures is chosen for the validation purposes because of their easy accessibility. The mass loss rate (MLR) data would be better to validate the pyrolysis model functionality; however, unlike the thermocouple temperatures mass loss rate data are not available from the standard RCT facility measurements. The temperature–time curve shows a rapid fire development in the first 50 s after the burner ignition. After the first 180 s, all model Scenarios, excluding Scenarios C and F, reach flashover and overestimate the experimentally measured temperatures by approximately

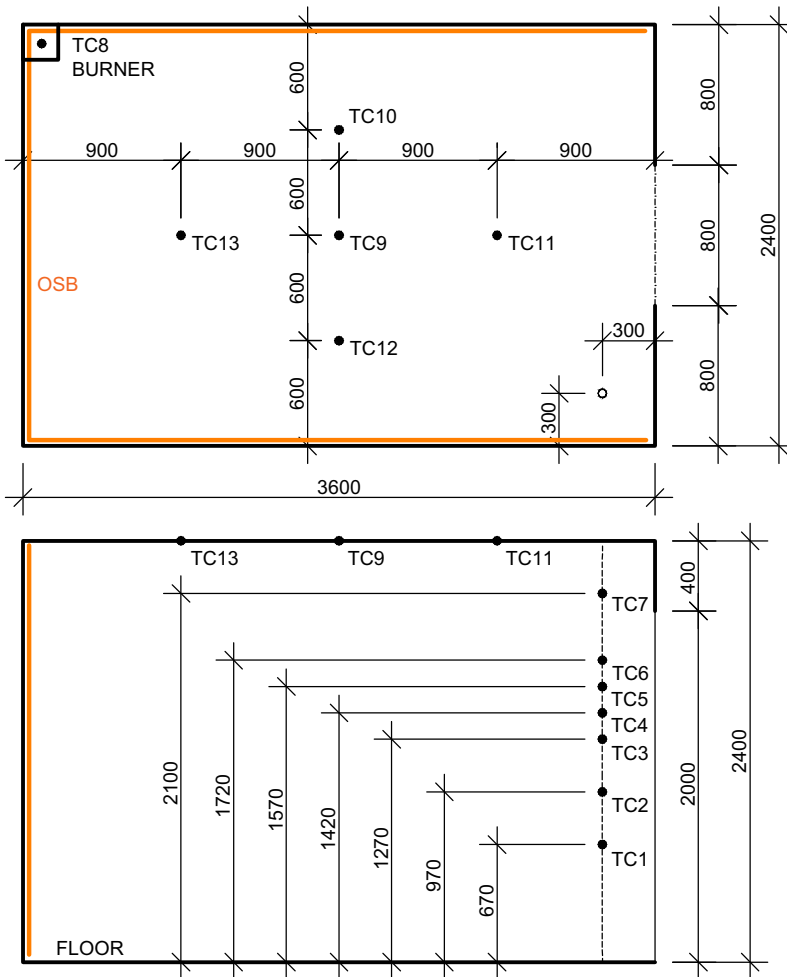


Figure 4.
Floor plan (upper
picture) and side cut
(lower picture) of the
fire test room including
positions of the
thermocouples (TC)
and walls covered
by OSB

200–600°C. On the contrary, in Scenarios C and F no fire development occurs, which is a consequence of involving water evaporation into a specific heat capacity temperature dependency. Scenarios C and F, therefore, underestimate the experimentally measured temperatures by approximately 100–350°C.

The experiment is interrupted at the time of 412 s (in Figure 6 marked with the grey vertical line labelled as burner shutdown). However, the models continue to predict the temperature development up to 1,800 s. The model predictions in all Scenarios A to G show the minimal dependency of model outputs on thermocouple location. This is probably the cause of early flashover and rapid temperature growth in the entire volume of the fire enclosure. Visualization of fire development during flashover is shown in Figure 7.

Scenario A, representing the most commonly used simplified model of burning, overestimates the experiment at any time more than any other model Scenario and reaches the maximum temperature of 1,360°C at 630 s. Scenarios B and G show nearly as high

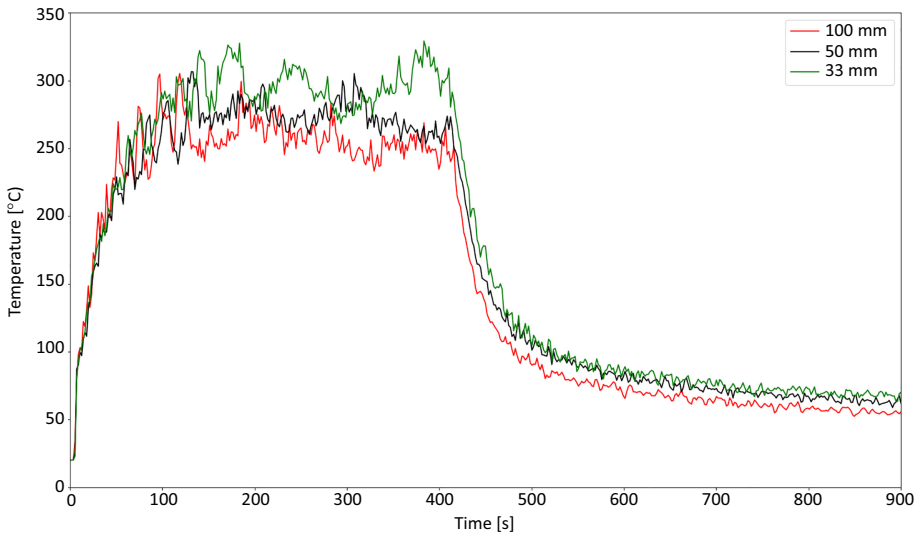


Figure 5.
Time-temperature
curve of thermocouple
TC7 for different
grid sizes

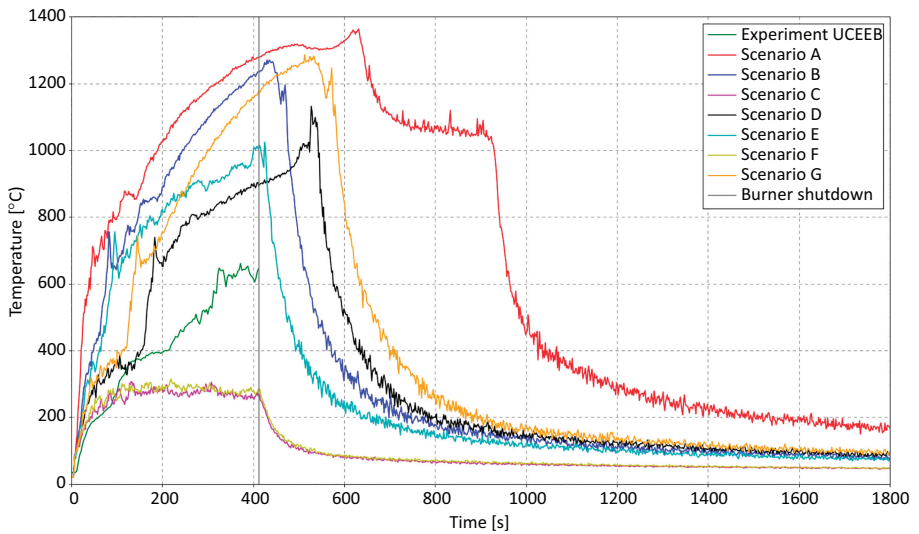


Figure 6.
Time-temperature
curve of
thermocouple TC7

over predictions as Scenario A reaching maximum temperature over 1,260°C. Model Scenario B reaches the maximum at roughly 430 s followed by a rapid temperature decrease. Model Scenario G reaches the maximum temperature followed by a rapid temperature decrease about 100 s later. The delay between model Scenarios B and G is a result of temperature-dependent specific heat capacity with neglected water evaporation introduced in Scenario G.

Model Scenarios D and E show that involving temperature-dependent heat conductivity lowers the maximum temperature by approximately 200°C in comparison to model Scenarios B and G (300°C in comparison to Scenario A). However, no significant shifts in the time of

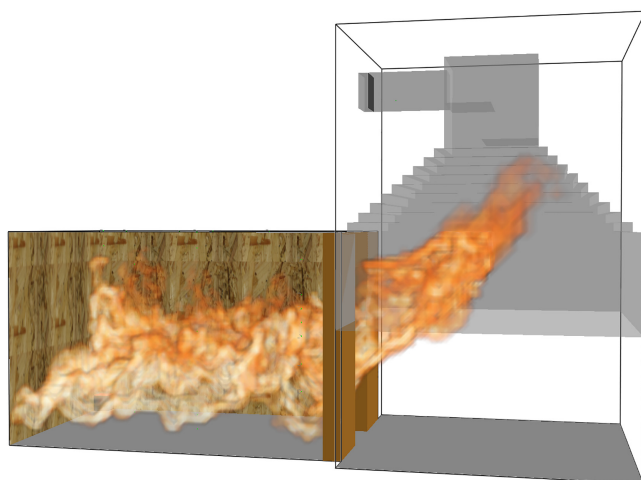


Figure 7.
The overview of model
Scenario D in
Smokeview at
time 180 s

maximum temperature occur. Approximately at the time of burner shutdown, model Scenario E reaches the lowest maximum temperature out of all other curves, which overestimate the experimental temperatures. Nevertheless, after the first 100 s, the best prediction of experimental data is achieved in model Scenario D.

In the case of Scenario A, the burnout occurs significantly later compared to other model Scenarios. In the range of 700–900 s, a roughly constant temperature of approximately 1,050°C is hold, followed by a rapid temperature decrease caused by reaching zero HRRPUA ramp values. In Scenario E, the temperature drops rapidly a couple of seconds after the burner shutdown. Scenarios B, D and G each follow the course of the rapid drop in Scenario E after 50 s, respectively. Generally, burnout is achieved after the burner shutdown followed by a rapid, approximately 100 s lasting temperature decrease reaching temperatures under 400°C.

The model's behaviour before the end of the experimental measurement and the differences in burning initiation and rapid acceleration of each model Scenario can be seen in [Figure 8](#). The figure shows significantly over predictions of the experimental temperatures at the very beginning of the simulation. Especially in the case of Scenarios A, B and E, where a constant specific heat capacity value is used, an extremely fast temperature increases up to approximately 400°C is recorded. The initial increase of temperature in the other model Scenarios is slightly slower. The best fit to experimental temperatures in the first 100 s is achieved in model Scenarios C and F, however, at approximately 100 s, the experimental curve starts to overpredict these two scenarios. In the interval of 100–160 s, the model Scenario D fits the experiment best. After the first 160 s, a substantial temperature increase of approximately 300°C occurs in model Scenario D, while the experimental temperature remains constant around 400°C. The temperature increase in Scenario D is caused by flames reaching the TC7 as flashover occurs. The experimental temperature starts to rise at 220 s following the course of Scenario D, which is shifted to higher temperatures by 250–300°C for the rest of the experimental record.

Scenarios C and F show the same course of the time–temperature curve throughout the entire simulation. This fact indicates that when water evaporation is added to the specific heat capacity, specific heat capacity becomes a dominant parameter. The effect of involving temperature-dependent heat conductivity becomes negligible. Both Scenarios C and F

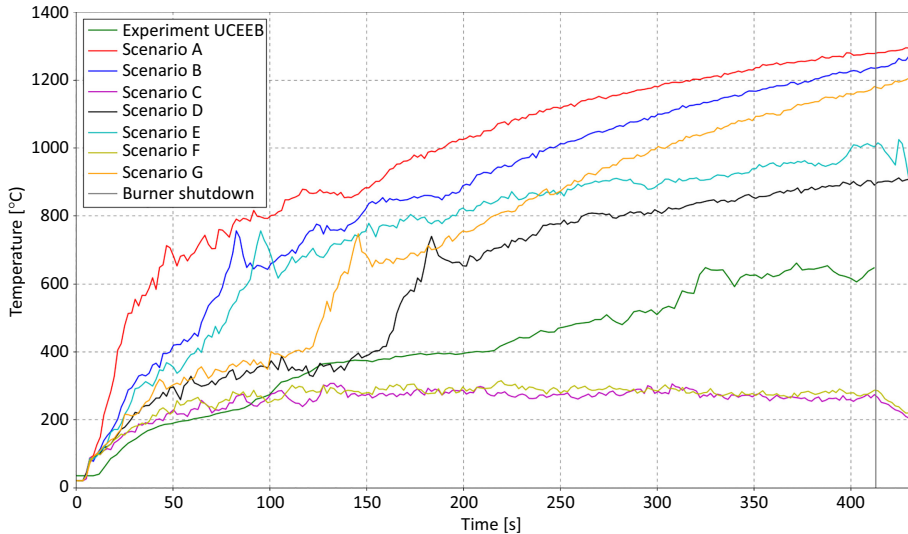


Figure 8.
Pre-flashover time–
temperature curve of
thermocouple TC7

maintain a constant temperature of roughly 300°C starting at approximately 100 s up to the burner shutdown. No flame development outside the space directly above the burner occurs.

TC7 temperature profile in [Figure 8](#) represents thermocouple behaviour in the hot layer. The other thermocouples TC5 and TC6 located in different heights in the hot layer show a very similar overall course in all model scenarios. The simulated TC5, TC6 and TC7 temperatures rise negligibly in the order of units to tens Celsius degrees as the height of thermocouples increases. The experimental TC5, TC6 and TC7 temperatures reached a higher difference up to 200°C, especially in the first 210 s. This fact reflects the effect of heat accumulation under the ceiling, where increasing thermocouple height leads to earlier thermocouple heating. This effect is significantly suppressed in simulations due to rapid heating and flames occurring in the whole hot layer space.

TC3 temperature profile in [Figure 9](#) represents thermocouple behaviour in the cold layer. Similarly to the hot layer, the cold layer thermocouples TC1, TC2 and TC3 predict the identical overall course and minimal temperature rise as thermocouples' height increases. In Scenarios C and F no flashover occurs, and the gaseous temperature in the cold layer does not exceed 50°C. The simulation outputs of all model Scenarios except Scenario C and F show a rapid step increase from room temperature to approximately 700°C as flashover flames hit the thermocouple. Due to the flashover occurrence in the simulations, the slow gradual heating of gaseous layers from the top to the bottom of the test room can be observed only in the experimental thermocouple data.

The simulation output of thermocouples TC8 and TC9 measuring the surface temperature above the burner and in the middle of the test room ceiling can be seen in [Figures 10](#) and [11](#), respectively. A slight shift of surface thermocouple temperature towards higher overall simulated temperatures (20–50°C for Scenarios C and F, 20–100°C for the other Scenarios) occurs compared to thermocouple at height 2,100 mm ([Figure 8](#)). In addition, the surface thermocouple located above the burner heats up earlier in comparison to other thermocouples due to flames reaching the ceiling. The effect of flames reaching the thermocouple significantly influences the course of temperature curves in model Scenarios C and F, where no other thermocouple reaches the temperature above 450°C. The transition into

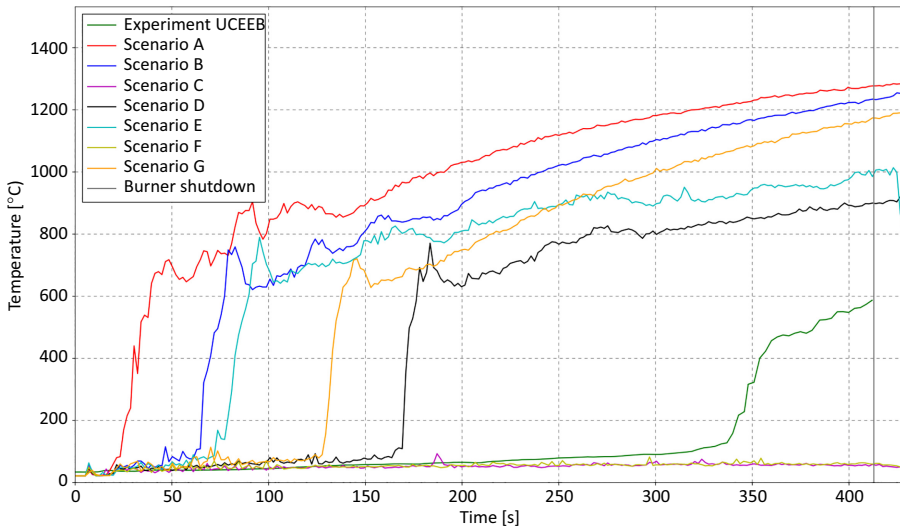


Figure 9.
Pre-flashover time-
temperature curve of
thermocouple TC3

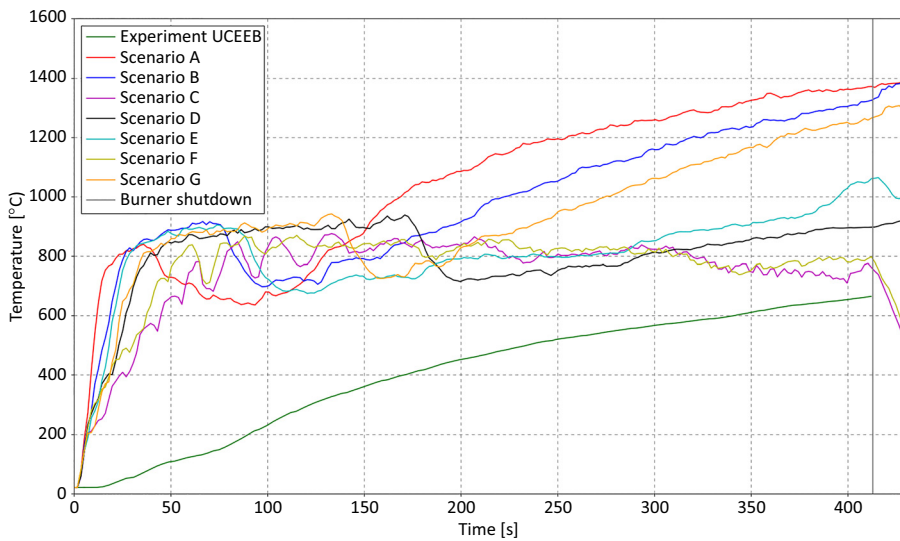


Figure 10.
Pre-flashover time-
temperature curve of
thermocouple TC8

ventilation-driven fire during flashover is illustrated by a temperature drop in Scenarios A, B, D, E and G, as the flames move from the ceiling towards the floor, doorway and under the hood (Figure 7).

4. Summary and recommendations

4.1 Numerical model of room corner test

A comparison of seven different FDS room corner test models covering simple to complex approaches with experiments showed the difficulty of modelling full-scale room scenarios, where fire spread and flashover occur and show the importance of a complete input

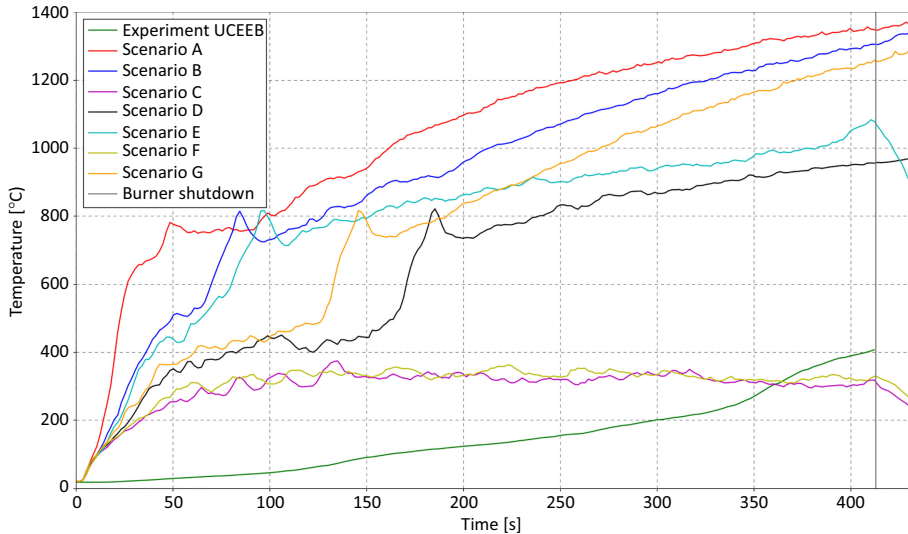


Figure 11.
Pre-flashover time-
temperature curve of
thermocouple TC9

parameters dataset. The results showed, in general, very little dependency of the model outputs on thermocouple location. This fact is attributed to the extremely rapid fire spread and heating of the entire interior space resulting in the early flashover during which flames reach all monitored thermocouples. The surface thermocouple located above the burner heated up earlier than other thermocouples due to flames reaching the ceiling. The other thermocouple temperatures increased in the order of units to tens Celsius degrees as the height of thermocouples increased. The difference between hot and cold layer thermocouples was noticeable only within approximately the first 120 s.

Apart from the standard mesh sensitivity analysis in the gaseous phase, the solid objects inner discretization was tested and changed from the default setting to prevent numerical instabilities. A test of solid object discretization and change to equidistant discretization with an increased number of computational points is highly recommended. Especially for materials undergoing thermal decomposition when using complex pyrolysis approach and/or temperature-dependent thermal properties.

The worst results were obtained in model Scenarios A, C and F. Scenario A, where the most common simplified model comprising HRRPUA input data was used, overestimated the experiment by 500–600°C reaching the maximum temperature of 1,360°C at 630 s. Thermocouple temperatures in Scenario A were overestimated at any time more than in any other model Scenario.

The complex approach Scenarios C and F were unique by including the water evaporation into temperature-dependent specific heat capacity. The poor outcome of Scenarios C and F is caused by preventing the fire spread from the space directly above the burner and thus preventing the subsequent flashover effect. As a result, Scenarios C and F underestimated the experiment by approximately 100–350°C reaching a very low maximum temperature of 300°C. The very similar outcome of Scenarios C and F indicates that when water evaporation is added into the specific heat capacity, specific heat capacity becomes a dominant parameter and the effect of involving temperature-dependent heat conductivity in Scenario C becomes negligible. Every other scenario, other than C and F, reached a flashover in the first 180 s.

Complex model Scenario B, where both constant specific heat capacity and thermal conductivity are used, shows an almost similar course of output temperatures compared to Scenario G. However, the temperatures in Scenario G are delayed by approximately 100 s throughout the entire simulation. The delay is a consequence of adding temperature-dependent specific heat with neglected water evaporation in Scenario G. Both Scenarios B and G reached the same maximum temperature over 1,260°C and overestimated the experimental temperature by approximately 450–550°C and 350–450°C, respectively.

Complex Scenario E, where constant specific heat capacity and temperature-dependent thermal conductivity were used, showed a more rapid temperature increase in the first 240 s compared to Scenario G. After 240 s, the temperature growth in Scenario E slowed resulting into significantly lower maximum temperature and lower experiment overestimation of approximately 300–400°C compared to Scenarios A, B and G. The maximum temperature of approximately 1,010°C in Scenario E was reached roughly at 412 s when the burner was shut down.

The best agreement with experimental data was achieved in complex Scenario D where both temperature-dependent thermal conductivity and specific heat capacity with neglected water evaporation are used. Scenario D showed the slowest initial temperature growth from all other scenarios and the lowest experiment temperature over predictions of a maximum of 300°C.

4.2 Recommendations to modelling approach and input parameters

In general, the simplified approach turned out to be the least suitable for modelling the room corner test. This model approach should be used with great care. A complex approach utilizing a large input dataset including three-step thermal decomposition kinetic parameters is needed to improve the model results when fire spread and flashover effect occurs. Besides the need for a complex approach, attention should be paid to the material thermal properties choice. A commonly used constant specific heat capacity and thermal conductivity provided poor agreement with experimental data. A much better result can be obtained by adding temperature-dependent thermal properties. The influence of adding evaporation of water into the specific heat capacity was also tested. It is not recommended to include water evaporation into specific heat capacity as it may prevent the fire from spreading outside the heat source. The more complex approach of adding water as a separate material which undergoes chemical reaction – evaporation should be further tested.

Obtaining a complete input dataset for the complex description of material burning is difficult and time-consuming but not impossible. A complete input dataset for the OSB is provided in this work. The use of a complex pyrolysis approach is recommended in real scale enclosure fire scenarios if possible, however, extra attention should be paid to burning materials thermal properties implementation. When the fire spread is expected, the simplified model results should be processed with great care and the user should be aware of possible significant errors.

The influence of thermal parameters should be further tested in the future. An optimization-based approach of obtaining thermal properties from small- and medium-size experiments may provide promising results. Other commonly used wooden based materials such as chipboard or plywood and virgin wood boards should be validated to real scale experiments in the future to confirm or disprove the need of a unique input dataset for each of these materials.

References

Beshir, M., Cicione, A., Wang, Y., Welch, S. and Rush, D. (2019), “Re-visiting NIST reduced/full-scale enclosure (R/FSE) experiments (2007-2008)”, *15th International Conference and Exhibition on*

- Fire Science and Engineering (Interflam 2019)*, Interscience Communications, London, pp. 2095-2107.
- Brunkhorst, S. and Zehfuss, J. (2020), "Experimental and numerical analysis of fire development in compartment fires with immobile fire load", in Makovicka Osvaldova, L., Markert, F. and Zelinka, S. (Eds), *Wood and Fire Safety, WFS 2020*, Springer, Cham. doi: [10.1007/978-3-030-41235-7_28](https://doi.org/10.1007/978-3-030-41235-7_28) (accessed 7 April 2021).
- Buchanan, A., Östman, B. and Frangi, A. (2014), "White paper on fire resistance of timber structures", Grant/Contract Reports (NISTGCR), National Institute of Standards and Technology, Gaithersburg. doi: [10.6028/NIST.GCR.15-985](https://doi.org/10.6028/NIST.GCR.15-985) (accessed 7 April 2021).
- Buchnarová, H. (2018), "Experimental detection of fire and heat technical characteristics of construction products and implementation of data into CFD models", Master thesis, CTU in Prague, Prague, available at: <https://dspace.cvut.cz/handle/10467/74113?locale-attribute=en> (accessed 7 April 2021).
- Drysdale, D. (2011), *An Introduction to Fire Dynamics*, 3rd ed., A John Wiley and Sons, Chichester, West Sussex.
- EN 1995-1-2 Eurocode 5 (2006), *Design of Timber Structures - Part 1-2: General - Structural Fire Design*.
- Gupta, M., Yang, J. and Roy, Ch. (2003), "Specific heat and thermal conductivity of softwood bark and softwood char particles", *Fuel*, Vol. 82 No. 8, pp. 919-927, doi: [10.1016/S0016-2361\(02\)00398-8](https://doi.org/10.1016/S0016-2361(02)00398-8) (accessed 7 April 2021).
- Hietaniemi, J., Hostikka, S. and Vaari, J. (2004), "FDS simulation of fire spread – comparison of model results with experimental data", working paper 4, VTT, Espoo, June 2004.
- Ira, J., Hasalová, L., Šálek, V., Jahoda, M. and Vystrčil, V. (2020), "Thermal analysis and cone calorimeter study of engineered wood with an emphasis on fire modelling", *Fire Technology*, Vol. 56, pp. 1099-1132, doi: [10.1007/s10694-019-00922-9](https://doi.org/10.1007/s10694-019-00922-9) (accessed 7 April 2021).
- ISO 9705-1 International Standard (2016), *Reaction to Fire Tests - Room Corner Test for Wall and Ceiling Lining Products - Part 1: Test Method for a Small Room Configuration*.
- Karlsson, B. (1992), "A mathematical model for calculating heat release in the room corner test", *Fire Safety Journal*, Vol. 20 No. 2, pp. 93-113, doi: [10.1016/0379-7112\(93\)90032-L](https://doi.org/10.1016/0379-7112(93)90032-L) (accessed 7 April 2021).
- Lattimer, B.Y., Luo, C., Kraft, S. and Hodges, J.L. (2019), "Rail car interior finish heat release rate requirements", *15th International Conference and Exhibition on Fire Science and Engineering (Interflam 2019)*, Interscience Communications, London, pp. 1317-1327.
- McGrattan, K., Hostikka, S., Floyd, J., McDermott, R. and Vanella, M. (2019a), *Fire Dynamics Simulator Technical Reference Guide Volume 1: Mathematical Model*, 6th ed., National Institute for Standards and Technology, Gaithersburg, MD, Special Publication 1018-1.
- McGrattan, K., Hostikka, S., Floyd, J., McDermott, R. and Vanella, M. (2019b), *Fire Dynamics Simulator User's Guide*, 6th ed., National Institute for Standards and Technology, Gaithersburg, MD, Special Publication 1019.
- Moghaddam, A.Z., Moinuddin, K., Thomas, I.R., Bennetts, I.D. and Culton, M. (2004), "Fire behaviour studies of combustible wall linings applying fire dynamics simulator", in Behnia, M., Lin, W. and McBain, G.D. (Eds), *15th Australasian Fluid Mechanics Conference*, The University of Sydney, Sydney, NSW, pp. 547-550.
- Moinuddin, K.A.M., Al-Menhali, J.S., Prasanna, K. and Thomas, I.R. (2011), "Rise in structural steel temperatures during ISO 9705 room fires", *Fire Safety Journal*, Vol. 46 No. 8, pp. 480-496, doi: [10.1016/j.firesaf.2011.08.001](https://doi.org/10.1016/j.firesaf.2011.08.001) (accessed 7 April 2021).
- Šálek, V. (2018), "Thermal characteristics of solid materials for modeling the spread of fires", Master thesis, UCT Prague, Prague, available at: <https://repozitar.vscht.cz/theses/27379/> (accessed 7 April 2021).
- Twilt, L. and Witteveen, J. (1974), *The Fire Resistance of Wood-Clad Steel Columns*, Fire Prevention Science and Technology, London, No. 11, pp. 14-20.

Weyerhaeuser (2018), “Weyerhaeuser Oriented Strand Board (OSB) products including: sheathing, Edge™, Edge Gold™, RBS™ (Radiant Barrier Sheathing), Rim Board, SturdiStep™”, available at: <https://www.weyerhaeuser.com/woodproducts/building-green-with-wood/product-stewardship-safety-data-sheets/> (accessed 7 April 2021).

Numerical
modelling of
fire test

Corresponding author

Vojtěch Šálek can be contacted at: salekv@vscht.cz

117

For instructions on how to order reprints of this article, please visit our website:

www.emeraldgrouppublishing.com/licensing/reprints.htm

Or contact us for further details: permissions@emeraldinsight.com